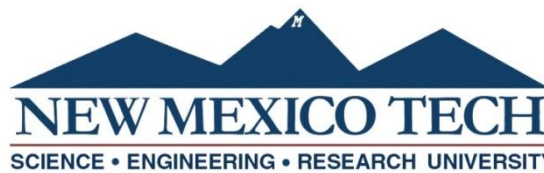


STEPWISE DYNAMIC CALIBRATION OF A HYDROMECHANICAL SIMULATION USING TIME- LAPSE VERTICAL SEISMIC PROFILE

by

Marcia D. McMillan

Submitted in Partial Fulfillment
of the Requirements for the Degree of
Doctor of Philosophy in Petroleum Engineering



New Mexico Institute of Mining and Technology
Socorro, New Mexico
December 2021

This thesis is dedicated to my mother for all their love and support throughout this process

Marcia D. McMillan
New Mexico Institute of Mining and Technology
December 2021

ABSTRACT

This study aims to develop a methodology for calibrating subsurface stress changes through time-lapse Vertical Seismic Profiling (VSP) integration. The selected study site is the 13-10A injector well within the ongoing CO₂-EOR operation of the Farnsworth Field Unit (FWU). Acquired time-lapse VSP, over the FWU CO₂-EOR process, carries the combined effects of fluid substitution and mean effective stress changes, thereby providing a dataset for calibrating production and injection-induced stress changes. The approach is similar to calibrating a reservoir simulation model. Actual field data is honored in structuring an inverse problem that solves for the optimal geomechanical input parameters. The resolved optimal geomechanical input parameters seek to replicate the observed time-lapse seismic velocity changes.

The stress calibration is enabled by 4D coupled hydromechanical modeling and the VSP Integration workflow, constructed in the seismic velocity domain. Seismic velocities attributed to fluid substitution and that due to stress change are linearly additive. The Biot Gassmann workflow combines the site-specific rock physics model and reservoir simulation outputs to determine the fluid substitution contribution to seismic velocity change. This project uses one calibrated reservoir simulation model, and thus the primary focus is on calibrating the geomechanical model. Modeled seismic velocities attributed to mean effective stress change are determined from the geomechanical simulation outputs and use the ultrasonic core measurements as the maximum velocity-stress derivative. A penalty function is then formed between the modeled seismic velocities and the observed time-lapse VSP dataset.

Four independent and impactful geomechanical parameters have been identified. These are the bulk modulus and shear modulus at zero porosity and the shear and compressional seismic velocity to mean effective stress derivatives. Randomly varying the independent geomechanical parameters and using them to build hydromechanical models generates a dataset suitable for optimization. A machine learning-assisted workflow comprised of an Artificial Neural Network (ANN) and a Particle Swarm Optimizer (PSO) are used to converge on the optimal geomechanical parameters.

Successful execution of this workflow has affirmed the suitability of acoustic time-lapse measurements for stress calibration. Application to other reservoirs and other operation schemes require measurable stress sensitivities over the anticipated range of stress changes and suitable datasets for petroelastic modeling.

Keywords: VSP Integration, Geomechanical Modelling, Optimization, CCUS

ACKNOWLEDGMENTS

First and foremost, I would like to express my sincere gratitude to my research advisor, Dr. William Ampomah, for his continued support during my Ph.D. studies. I have benefitted greatly from his generosity, demonstrated by the straightforward way he has shared his copious geomechanical knowledge and Petrel skills. I offer a special thank you to Dr. Hassan Khaniani for his tirelessness in deepening the technical quality of my research. I am also extremely grateful to my academic advisor Dr. Thomas Engler and my entire Ph.D. committee: Dr. Her-Yuan Chen, Dr. William Ampomah, and Dr. Hassan Khaniani, for sharing their enormous knowledge, time, patience, and support.

My sincere thanks to Dr. Tom Bratton, Mr. Don Lee, Dr. Robert Will, Dr. Huang Liange, and Mr. George El-Kaseeh for their invaluable inputs, expert knowledge, and guidance. I also owe a significant debt of gratitude to Dr. Robert Will for his advice and the investment of his time. My sincere thanks go to Dr. Robert S. Balch, the Petroleum Recovery Research Center Director, and the Reservoir Evaluation and Advanced Computational Technologies (REACT) Group. Your comments, inputs, suggestions, and inciteful questions have improved the quality of my research.

I also want to thank the U.S. Department of Energy's (DOE) National Energy Technology Laboratory (NETL) DOE Award No. DE-FE31684 for funding this project and the associated Southwest Regional Partnership on Carbon Sequestration (SWP) under DOE Award No. DE-FC26-05NT42591. I am also grateful for the support provided by the site operator Perdure Petroleum, L.L.C., and Schlumberger Carbon Services.

I also thank the entire faculty and staff of the Petroleum Engineering Department at NMT for their support and encouragement. I also thank my fellow students for adding life, color, and humor to my time at NMT.

Last but not least, my special thanks go to my entire loving family and friends who have continuously encouraged me. Finally, I am very grateful to the Almighty God for his blessings and mercies throughout these years.

TABLE OF CONTENTS

ABSTRACT	iv
ACKNOWLEDGMENTS	iv
LIST OF TABLES	viii
LIST OF FIGURES	ix
LIST OF ABBREVIATIONS AND SYMBOLS	xii
CHAPTER 1	1
INTRODUCTION	1
1.1 Statement of Purpose	2
1.1.1 Study area.....	2
1.1.2 Workflow Description	2
1.2 Research Objective and Major Contribution of this Thesis	3
1.3 Organization of Thesis	3
CHAPTER 2	5
LITERATURE REVIEW	5
2.1 4D Geomechanical Calibration	6
2.2 Stress and Strain, Concepts of Seismic Velocity Change	8
2.2.1 Linking Stress, Strain, and Seismic Wave Velocity	8
2.2.2 Seismic Velocity: Impacts of Fluid Substitution	9
2.2.3 Krief model Rockframe Elastic Moduli.....	10
2.2.4 Seismic Velocity to Mean Effective Stress: Impacts of Pore Pressure Change ..	11
2.3 Quantitative Utilization of Seismic Data	12
2.4 Calibration Techniques	12
2.4.1 Reservoir Simulation Calibration	13
2.4.2 Geomechanical Parameter Optimization	13
2.4.3 Artificial Neural Network	13
2.4.4 Particle Swarm Optimization.....	14
2.4.5 Hybrid Machine Learning Workflow	15
2.5 Literature Review Summary	17
CHAPTER 3	18
FARNSWORTH FIELD UNIT BACKGROUND	18
3.1 Morrow B Background	18
3.2 Field Operational History and Production	20
3.3 Specialized Studies and Impetus for FWU Geomechanics	21
CHAPTER 4	23
VSP INTEGRATION METHODOLOGY AND REQUIRED DATASETS	23
4.1 Overview	23
4.2 VSP Study Area and VSP Acquisition	24
4.2.1 Time-Lapse VSP Dataset.....	26
4.3 Time-Lapse Seismic Velocity Attributed to Fluid Substitution	30
4.3.1 Compositional Reservoir Simulation.....	30
4.3.2 Site-Specific Rock Physics Model.....	30
4.3.3 Seismic Velocity Attributed to Fluid Substitution.....	32
4.4 Time-Lapse Seismic Velocity Change Due to Stress	32
4.4.1 Geomechanical Simulation Model Linear Elastic Assumption	32

4.4.2 Ultrasonic Measurement of Core	33
4.4.3 Effective Stress and Seismic Velocity	37
4.5 Formulation of Objective Function	37
4.5.1 Linear Summation.....	37
4.5.2 Backus Averaging.....	37
4.5.3 Formulation of Penalty Function	38
4.6 Optimization Workflow.....	39
4.6.1 Design of Experiments (DOE) and Independent Parameters	39
4.6.2 Independent Fluid Substitution Parameterization	39
4.6.3 Geomechanical Parameterization.....	39
4.6.4 Deterministic and Stochastic Analysis.....	40
4.7 Critical Factors for Workflow Execution.....	41
4.8 Datasets and Integration Summary	41
CHAPTER 5.....	43
COUPLED GEOMECHANICAL MODELS: CONSTRUCTION,	
INITIALIZATION AND DYNAMIC TESTING	43
5.1 Introduction.....	43
5.2 Workflow Overview of Mechanical Earth Model Construction	44
5.2.1 Geologic Model	44
5.2.2 Hydrodynamic Properties and Reservoir Simulation	44
5.3 Geomechanical Model Construction	45
5.4 Coupling Procedures	48
5.5 Stress Initialization	49
5.5.1 Horizontal Stress Magnitude and Orientation.....	49
5.5.2 Geomechanical Stress Boundary Condition	51
5.5.3 Stress State Diagram	51
5.5.4 Mohr-Coulomb Stress State Evaluation.....	54
5.6 Dynamic Modeling.....	55
5.6.1 Permeability updates.....	55
5.6.2 Coupled Primary & Secondary Production Stress Changes.....	57
5.6.3 CO ₂ -WAG Stress Changes, (December 2010 to July 2017).....	58
5.7 Chapter Summary	60
CHAPTER 6.....	62
STRESS CALIBRATION	62
6.1 Introduction.....	62
6.2 Pertinent Theory	63
6.3 Results and Discussion.....	63
6.3.1 Calibrated Reservoir Simulation Model	63
6.3.2 Modeled Time-Lapse Seismic Velocity due to Stress	64
6.3.3 Comparison of Base Case and Observed Dataset	66
6.3.4 Geomechanical Optimization: Deterministic Analysis: Sensitivity Analysis	67
6.3.5 Deterministic Solution Surfaces	69
6.3.6 Stochastic Evaluation.....	70
6.3.7 Optimization	72
6.4 Examination of Optimized Result	74
6.4.1 Modeled Seismic Velocity Attributed to Fluid substitution	75

6.4.2 Modeled Seismic Velocity Due to Stress Change	78
6.5 Chapter Summary	82
CHAPTER 7	84
CONCLUSIONS AND FURTHER WORKS.....	84
7.1 Conclusions.....	84
7.2 Further Work	85
REFERENCES.....	87
APPENDIX A: WORKFLOW VERIFICATION	96

PREVIEW

LIST OF TABLES

Table	Page
TABLE 3.1: BASIC MORROW B RESERVOIR PROPERTIES.....	19
TABLE 6.1: BASE CASE PROPERTIES FOR SENSITIVITY ANALYSIS	66
TABLE 6.2: TABULATED PARAMETER OBJECTIVE FUNCTION EXTREMES FOR SENSITIVITY ANALYSIS	68
TABLE 6.3 SUMMARY OF OPTIMIZED GEOMECHANICAL PARAMETERS AND ASSOCIATED ERROR	74

PREVIEW

LIST OF FIGURES

Figure	Page
FIGURE 2.1: PARTICLE SWARM OPTIMIZATION ALGORITHM	15
FIGURE 2.2 MACHINE LEARNING ASSISTED WORKFLOW IMPLEMENTED FOR GEOMECHANICAL CALIBRATION	17
FIGURE 3.1: PROVIDES A GEOGRAPHICAL REFERENCE FOR THE SOUTHWEST REGIONAL PARTNERSHIP ON CO ₂ SEQUESTRATION, THE ANADARKO BASIN AND FARNSWORTH FIELD UNIT (FWU). THE HIGHLIGHTED REGION IS MAGNIFIED TO ILLUSTRATE THE SOURCES OF CO ₂ AND THE CONNECTING PIPELINE INFRASTRUCTURE (FWU).	19
FIGURE 3.2: STRATIGRAPHIC COLUMN FOR FARNSWORTH FIELD UNIT.....	20
FIGURE 3.3: MORROW B PRESSURE AND PRODUCTION HISTORY WITH THE PRODUCTION METHODOLOGIES ARE HIGHLIGHTED.	21
FIGURE 4.1: OVERVIEW OF VSP INTEGRATION AND OPTIMIZATION WORKFLOW	25
FIGURE 4.3: TIME SLICE OF INVERTED SHEAR AND COMPRESSIONAL SEISMIC VELOCITY. VSP INVERSION IS PERFORMED BY LOS ALAMOS NATIONAL LABS.	28
FIGURE 4.4: CROSS SECTION THROUGH TIME-LAPSE SHEAR AND COMPRESSIONAL SEISMIC VELOCITY CROSSING THE 13-6, 13-14, AND 13-10A	29
FIGURE 4. 5: DEVELOPMENT OF KRIEF ROCK PHYSICS RELATIONSHIP FOR MORROW-B FORMATION SHOWS THE A) SHEAR MODULUS VERSUS POROSITY, WHILE B) SHOWS THE BULK MODULUS.....	31
FIGURE 4. 6: ULTRASONIC SEISMIC RESPONSE OF CORE DIRECTLY CORRELATES MEAN EFFECTIVE STRESS CHANGES AND CHANGES IN SHEAR AND COMPRESSIONAL SEISMIC VELOCITY. CORES SUITABLE FOR LABORATORY TRIAXIAL ULTRASONIC VELOCITY MEASUREMENTS MUST BE WHOLE AND UNBROKEN. DUE TO THEIR SMALL SIZE (INCHES), THEY ARE LIKELY TO BE FREE OF COMPLIANCES AND THUS REPRESENT THE MAXIMUM VALUE OF THE SEISMIC VELOCITY TO MEAN EFFECTIVE STRESS.	34
FIGURE 4. 7: MORROW B ELASTIC MODULI	36
FIGURE 5.1: BLOCK DIAGRAM OF MECHANICAL EARTH MODELING WORKFLOW APPLIED AT FWU	45
FIGURE 5.2: CONSTRUCTED GEOLOGICAL FRAMEWORK WITHIN THE SECTOR BOUNDARY. X AND Y DIRECTION SLICES THROUGH THE MODEL SHOWING MAIN ZONES AND SUB-LAYERS FOR EACH ZONE. (LEFT).	46
FIGURE 5. 3: SEISMIC INVERSION DERIVED ESTIMATE OF YOUNG MODULUS IN THE MORROW B AND (B) DISTRIBUTION-ADJUSTED AND CO-KRIGED MORROW B YOUNG MODULUS IN THE GEOMECHANICAL GRID.	47
FIGURE 5. 4: VISUALIZATION OF EMBEDDED RESERVOIR SIMULATION GRID WITHIN THE GEOMECHANICAL GRID	48
FIGURE 5. 5: A) FULL WELLBORE STRESS INITIALIZATION AND B) ZOOMED-IN ASSESSMENT OF THIRTEEN FINGER TO MORROW D. BOTH DIAGRAMS SHOW A GOOD COMPARISON BETWEEN MODELED STRESS INITIALIZATION (MULTI-COLORED SOLID BARS) AND THE 1D MEM PARAMETERS (MULTI-COLORED LINES) THAT INFORM THE GEOMECHANICAL MODELING. ...	53

FIGURE 5. 6: STRESS STATE DIAGRAM ILLUSTRATES ALL POSSIBLE STRESS STATES FOR DEPTH AND PORE PRESSURE. ALLOWABLE STRESS STATES ARE FURTHER CONSTRAINED BY DRILLING INDUCED TENSILE FRACTURES AND BOREHOLE BREAKOUTS LEAVING ONLY THE PURPLE HASHED AREA. GEOMECHANICAL MODEL IS INITIALIZED (RED DIAMOND) AT OVERBURDEN GRADIENT OF 1.093 PSI/FT, $SH_{MIN} = 0.85$ PSI/FT, $SH_{MAX} = 0.92$ PSI/FT AND A PORE PRESSURE GRADIENT OF 0.586 PSI/FT, WHICH FALLS IN THE NORMAL FAULTING REGION.	54
FIGURE 5. 7: PERMEABILITY CHANGES DUE TO VOLUMETRIC STRAIN, COMPUTED USING KOZENY-CARMAN RELATIONSHIP FOR THREE DIFFERENT POROSITY -PERMEABILITY COMBINATIONS	55
FIGURE 5. 8: COMPARISON OF FIELD PRESSURE (SOLID LINE) AND CUMULATIVE OIL PRODUCTION (DASHED LINE) DURING THE PRIMARY AND WATERFLOOD RECOVERY PERIOD FOR NO-PERMEABILITY UPDATE (BLACK), ONE-YEAR PERMEABILITY UPDATE (GREEN), FIVE-YEAR PERMEABILITY UPDATE (BLUE), AND TEN-YEAR PERMEABILITY UPDATE (ORANGE)	56
FIGURE 5. 9: COMPARISON OF FIELD PRESSURE (SOLID LINE) AND CUMULATIVE OIL PRODUCTION DURING THE CO ₂ -WAG PERIOD FOR NO-PERMEABILITY UPDATE (BLACK), THREE-MONTH PERMEABILITY UPDATE (GREEN), AND ONE-YEAR PERMEABILITY UPDATE (BLUE).	57
FIGURE 5. 10: A) STRESS CHANGES DURING PRIMARY PRODUCTION INDICATE INCREASED PORE PRESSURE AND A SLIGHT INCREASE IN MOHR CIRCLE SIZE. FIGURE 5.10B) ILLUSTRATES THE STRESS EFFECTS DURING THE SECONDARY RECOVERY- WATERFLOOD PERIOD: EFFECTIVE STRESSES AND MOHR CIRCLE SIZE DECREASE DUE TO THE INCREASING PORE PRESSURE	59
FIGURE 5. 11: MOHR CIRCLES SHOWS STRESS CHANGES IN THE MORROW B THROUGHOUT THE WAG CYCLES.	60
FIGURE 6. 1: CALIBRATED RESERVOIR SIMULATION COVERING THE TIME-LAPSE VSP STUDY PERIOD.	64
FIGURE 6. 2: IDENTICAL STRESS DISTRIBUTION FOR FULL FIELD (SOLID COLORED BARS) AND THE SECTOR MODEL (DASHED ORANGE OUTLINE).....	65
FIGURE 6. 3: TIME-LAPSE COMPRESSIONAL SEISMIC VELOCITIES, LARGE MEAN SQUARE DIFFERENCES BETWEEN OBSERVED (TOP) AND MODELED (BOTTOM) INDICATE THE NEED FOR OPTIMIZATION. MONITOR 1, 2 AND 3 ARE SHOWN.....	66
FIGURE 6. 4: TIME-LAPSE SHEAR SEISMIC VELOCITIES, LARGE MEAN SQUARE DIFFERENCES BETWEEN OBSERVED (TOP) AND MODELED (BOTTOM) INDICATE THE NEED FOR OPTIMIZATION. MONITOR 1, 2 AND 3 ARE SHOWN.....	67
FIGURE 6. 5: SENSITIVITY ANALYSIS FOR IMPACTFUL AND INDEPENDENT GEOMECHANICAL PARAMETERS. THE COMPRESSIONAL SEISMIC VELOCITY TO STRESS DERIVATIVE IS THE MOST IMPACTFUL PARAMETER, FOLLOWED BY THE G_{SMEAN} , THE $dV_s/d\Sigma'$ AND LASTLY THE K_{SMEAN}	69
FIGURE 6. 6: SOLUTION SURFACE FOR VARIATIONS IN M_{SMEAN} AND K_{SMEAN} PLOT SHOWS A MINIMUM VALUE AT $M_{SMEAN} = 3.0$ MPSI AND $K_{SMEAN} = 3.474$ MPSI. B) SOLUTION SURFACE FOR VARIATIONS IN $dV_p/d\Sigma'$ AND $dV_s/d\Sigma'$. MINIMA APPARENT AT $dV_p/d\Sigma' = 57.1$ M/S AND $dV_s/d\Sigma' = 53.1$ M/S PER 1000 PSI CHANGE IN MEAN EFFECTIVE STRESS.	70
FIGURE 6. 7: TOP-LEFT: FIRST ORDER, TOP-RIGHT: SECOND ORDER, BOTTOM LEFT: ARTIFICIAL NEURAL NETWORK AND BOTTOM RIGHT: COMPILATION PLOT FOR THE TOTAL OBJECTIVE FUNCTION. EACH GRAPH INDICATES THE MEAN SQUARE ERROR (MSE) AND THE R^2	

(COEFFICIENT OF DETERMINATION) AS MEASURES OF THE GOODNESS OF FIT. THE ANN PROVIDES THE BEST CORRELATION.	72
FIGURE 6. 8: SNAPSHOTS OF SATURATION WITHIN THE COMPOSITIONAL RESERVOIR SIMULATION SECTOR MODEL AT BASELINE, MONITOR 1, MONITOR 2, AND MONITOR 3. SATURATION CHANGES DRIVE MODIFICATIONS IN SHEAR AND COMPRESSIONAL SEISMIC VELOCITIES. ...	75
FIGURE 6. 9: TIME-LAPSE CHANGES IN FORMATION BULK DENSITY (TOP) AND TIME-LAPSE CHANGES IN SHEAR-SEISMIC VELOCITY FOR EVERY MONITOR TIME-STEP (RELATIVE TO VSP BASELINE).	76
FIGURE 6. 10: SHOWS THE CORRELATION BETWEEN TIME-LAPSE CHANGES IN BULK MODULUS OF THE PORE-FILLING FLUID (TOP) AND THE COMPRESSIONAL TIME-LAPSE SEISMIC VELOCITY (RELATIVE TO VSP BASELINE) FOR MONITORS 1, 2, AND 3 (BOTTOM ROW). THE FORMATION BULK DENSITY CHANGE, AND FLUID BULK MODULUS BALANCE DRIVE THE RESULTING COMPRESSIONAL SEISMIC VELOCITY CHANGE.	77
FIGURE 6. 11: EFFECTIVE STRESS CHANGES OUTSIDE OF THE MORROW B FORMATION ARE SMALL IN PART BECAUSE THE RESERVOIR SIMULATION USED ZERO POROSITY AND PERMEABILITY IN THE OVERLYING AND UNDERLYING FORMATIONS. THE TIME-LAPSE DIFFERENCES ARE DUE SOLELY TO STRESS REDISTRIBUTION.	78
FIGURE 6. 12: TIME-LAPSE SEISMIC VELOCITY CHANGES DUE TO STRESS AT EVERY MONITOR TIME WITHIN A 1000 FT RADIUS OF THE 13-10A WELL. THE TOP SHOWS THE COMPRESSIONAL SEISMIC VELOCITY. THE BOTTOM SHOWS THE SHEAR SEISMIC VELOCITY.	79
FIGURE 6. 13: TIME-LAPSE SHEAR SEISMIC VELOCITY CHANGES. ROW 1 PRESENTS THE OBSERVED DATASET, AND ROW 2 REPRESENTS THE MODELED SHEAR SEISMIC VELOCITY. .	80
FIGURE 6. 14: TIME-LAPSE COMPRESSIONAL SEISMIC VELOCITY CHANGES. ROW 1 PRESENTS THE OBSERVED DATASET, AND ROW 2 REPRESENTS THE MODELED COMPRESSIONAL SEISMIC VELOCITY.	81
FIGURE 7.1 OVERVIEW OF VSP INTEGRATION AND OPTIMIZATION WORKFLOW	86

LIST OF ABBREVIATIONS AND SYMBOLS

NMT	New Mexico Tech
FWU	Farnsworth Field Unit
SWP	Southwest Regional Partnership on CO ₂ Sequestration
EOR	Enhanced Oil Recovery
WAG	Water Alternating Gas
CO ₂	Carbon Dioxide
BHP	Bottom Hole Pressure
VSP	Vertical Seismic Profile
CCS	Carbon Capture and Storage
CCUS	Carbon Capture, Utilization and Storage
ANN	Artificial Neural Network
PSO	Particle Swarm Optimization

The dissertation is accepted on behalf of the faculty Institute by the following committee:

Dr. Thomas Engler

Academic Advisor

Dr. William Ampomah

Research Advisor

Dr. Her-Yuan Chen

Committee Member

Dr. Hassan Khaniani

Research Advisor

I release this document to the New Mexico Institute of Mining and Technology.

Marcia D. McMillan

11/29/2021

Chapter 1

INTRODUCTION

The criticality of the current climate crisis has prompted the International Energy Agency (IEA) to develop greenhouse gas (GHG) emission reduction scenarios to minimize CO₂ atmospheric concentrations while ensuring reliable and affordable access to energy and continued economic growth (Rubin et al., 2005). The 2013 IEA scenario for an 80% chance of limiting global temperature rise to 2°C by 2050 requires a 14% contribution from Carbon Capture and Storage (CCS) (IEA, 2013).

CCS encompasses the capture, transportation, and storage of CO₂, while in CCUS (Carbon Capture Utilization and Storage), the captured CO₂ is utilized beneficially. A prominent example of CCUS is CO₂-EOR (CO₂-Enhanced Oil Recovery) flooding. CO₂-EOR was first implemented in SACROC West Texas to increase oil recovery (Dicharry et al., 1973) and is now recognized as a valid CO₂ sequestration endeavor if a closed-loop system and appropriate MVA (Monitoring Verification Accounting) processes are implemented. In addition, the current Q45 tax incentive for CO₂ utilization (Grant 2019) only increases interest in CCUS techniques.

The injection and storage of large volumes of CO₂ in the subsurface, associated with CCS and CCUS, increase the geomechanical risks. Many monitoring and verification procedures are implemented to ensure the safe, reliable and permanent storage of CO₂. The IEAGHGT report (IEAGHGT, 2020) recounts and ranks many techniques and identifies examples of their implementation.

Cited examples include In Salah, a well-known industrial-scale CCS project that has utilized InSAR (Interferometric Synthetic Aperture Radar) technologies to measure overlying surface deformation (Morris et al., 2011; Ringrose et al., 2013; Rutqvist et al., 2010). The Weyburn CO₂-EOR demonstration project identified leakage from legacy wells as the most significant potential risk for containment loss. Another monitoring method is time-lapse VSP which aids in the delineation of the developing CO₂ plume. VSP is a wellbore seismic technique in which either the source or the receivers are located in the wellbore. Numerical coupled hydromechanical simulation models, informed by site-specific geomechanical evaluations, are also used to assess geomechanical risks.

It is widely recognized that time-lapse seismic carries the combined effects of changes in the physical states, including fluid substitution and stress changes. Understanding the stress state is critical for assessing the activation of potential leakage pathways and providing containment assurance. This dissertation combines coupled hydromechanical modeling with acquired time-lapse VSP to calibrate subsurface stress changes.

The production and operation dataset used for this study is from the ongoing CO₂-EOR operations at FWU, and the acquired time-lapse VSP dataset is reported by El-Kaseeh (El-kaseeh et al., 2018). The FWU is part of the Department of Energy (DOE) Demonstration Project for the Southwest Regional Partnership on CO₂ Sequestration (SWP). The DOE and National Energy Technology Laboratory (NETL) provide funding for both SWP and this associated stress calibration study.

1.1 Statement of Purpose

The complexity of stress states at even a single point requires the full complement of principal stresses, directional cosines, and pore pressure (Dusseault et al., 2007). Stress magnitude cannot be measured directly and require indirect stress indicators such as Diagnostic Fracture Injection Test (DFIT), full-field 3D seismic and Vertical Seismic Profiles. The datasets used in this study include time-lapse VSP with pressure and temperature monitoring at the injection well. The time-lapse measurements are repeated at intervening times over the same geographical region. These datasets provide tremendous benefits, representing snapshots of the reservoir condition, which inherently incorporate the stress state effects (Lumley, 2001).

This work combines a time-lapse VSP dataset with numerical modeling to achieve a dynamic 4D hydromechanical stress calibration. While the concept of 4D geomechanical calibration is not entirely new (Olden et al., 2001; Verdon et al., 2011), no published literature has been found describing time-lapse VSP over a CO₂-EOR operation utilized for subsurface stress calibration. The ability to successfully calibrate the hydromechanical model using the time-lapse VSP dataset extends its utility. Furthermore, calibration with actual field data increases confidence in stress predictions, and the concept can be applied to other CCS, CCUS and thermal operations.

1.1.1 *Study area*

The hydromechanical calibration procedures are demonstrated using field data and models from the Farnsworth West Unit (FWU). FWU development began in 1955 with primary depletion followed by an extensive period of water flooding, commencing in 1964 and continuing until the phased implementation of CO₂-WAG (Water Alternating Gas) EOR in 2010. As of August 2020, the FWU has permanently stored 1.38×10^6 million tonnes (Mt) of CO₂. FWU must permanently sequester these large volumes of CO₂. The current average reservoir pressure is estimated at greater than twice the reservoir pore pressure at discovery, though initially under-pressured, introducing significant concerns over storage containment integrity.

1.1.2 *Workflow Description*

This work demonstrates a 4D hydromechanical calibration by ground-truthing modeled time-lapse seismic velocity against an acquired Vertical Seismic Profile (VSP) datasets inverted to give time-lapse seismic velocities. For FWU CO₂-EOR operations, causes of seismic velocity changes are attributed either to fluid substitution or the changes in mean effective stress, which are treated as linearly additive.

Seismic velocity changes attributed to fluid substitution are computed using the Biot-Gassmann workflow and require fluid property outputs from the reservoir simulation along with a site-specific Krief rock physics model. Only one deterministic reservoir simulation model calibration is used in this study. Modeled time-lapse seismic velocity due to changes in stress are computed from the effective stress outputs of the geomechanical simulation and use the seismic velocity–stress derivative from ultrasonic testing on the core as the maximum stress sensitivity.

The calibration procedures are enabled through a machine learning-assisted computational workflow which combines an Artificial Neural Network (ANN) with a Particle Swarm Optimization (PSO). This novel integrated workflow utilizes datasets from the ongoing CO₂-EOR operation in Farnsworth Field Unit (FWU).

Successful workflow execution effectively calibrates subsurface hydromechanical changes for production and injection-induced stress effects and potentially augments procedures for assessing subsurface stress changes.

1.2 Research Objective and Major Contribution of this Thesis

The research objective is to construct a VSP Integration workflow that enables dynamic stress calibration during the active CO₂-EOR operations within the Farnsworth Field Unit. This objective is achieved through the following sequence.

- (1) Construct a static 3D Mechanical Earth Model (MEM) for the Farnsworth Field Unit based on full-field 3D seismic, 3D seismic inversion, structure, stratigraphy, well logs and the 1D MEM on the 13-10A characterization well. The 13-10A injector is the central focus of the VSP integration workflow.
- (2) Build a dynamic coupled hydromechanical simulation model and test for production and injection-induced stress effects within the Morrow B.
- (3) Evaluate the relative impacts on pore pressure and stress effects predicted by one-way coupling versus 2-way coupling.
- (4) Construct the VSP integration workflow. VSP integration workflow uses the reservoir simulation outputs to compute the modeled seismic velocity changes attributed to fluid. Additionally, changes in mean effective stress calculated in the geomechanical model are directly correlated to changes in seismic velocity from ultrasonic measurements on the core. Reconciling differences in scale between seismic scale (observed VSP) and reservoir scale (numerical simulation), the observed time-lapse seismic velocity is differenced from modeled seismic velocities at every time-lapse time-step to formulate the objective function.
- (5) A Machine Learning Assisted workflow is applied to minimize the objective function and calibrate the geomechanical input parameters, assessing the relative contributions of stress changes and fluid substitution on the seismic velocity changes.

1.3 Organization of Thesis

This dissertation consists of 6 additional chapters (excluding the current introductory chapter).

Chapter 2 is the literature review. Recent publications outlining the 4D geomechanical calibrations are reviewed. The links between geomechanics and seismic velocity and the underlying theory of how fluid substitution and changing stress induce seismic velocity change are addressed, followed by the reconciliation of scales for quantitative seismic

integration. Finally, the machine learning algorithms used for hydro-mechanical optimization are addressed.

Chapter 3 addresses the Farnsworth Field background and the impetus for and geomechanical evaluation

Chapter 4 presents the methodology for the VSP integration workflow, interlaced with the specialized datasets that reduce the uncertainty of the VSP integration workflow.

Chapter 5 describes the building and initialization of the 3D Mechanical Earth Model based on the 1D MEM conducted in January 2014. The result of dynamic testing of the coupled model is also presented.

Chapter 6 presents the results of the VSP integration workflow. The calibrated reservoir simulation model and the base case for the geomechanical model are presented. The deterministic and stochastic studies of the independent geomechanical parameters follow. Chapter 6 presents the calibration of the hydro-mechanical simulation model using linear and second-order mapping functions, followed by the ANN. The chapter concludes with the optimized result from the Machine Learning Assisted Workflow

Chapter 7 provides the concluding statements and recommendations for further work.

Chapter 2

LITERATURE REVIEW

This study performs the stepwise calibration of a coupled hydro-mechanical simulation model through a Vertical Seismic Profile (VSP) integration workflow. This is a case study of the active CO₂-EOR operations at Farnsworth Field Unit (FWU) in Ochiltree County, Texas. The observed VSP dataset is inverted to give shear and compressional seismic velocities at the baseline and three (3) monitor times, generating three (3) pairs of time-lapse seismic velocities, each relative to the baseline. The VSP integration workflow attributes seismic velocity changes to fluid substitution and to changes in mean effective stress only.

Hydro-mechanical calibration is the selection of input reservoir simulation and geo-mechanical parameters which best duplicate the dataset being matched. The calibration procedure is referred to as stepwise because the compositional reservoir simulation is calibrated before the one-way coupling with the geomechanical arm of the hydromechanical simulation model. The stress calibration is performed in the velocity domain, utilizing the modeled seismic velocities due to fluid substitution (from the reservoir simulation model) and due to mean effective stress change (geomechanical model). Reservoir simulation calibration is a well-established inverse problem that determines the independent and impactful reservoir and petrophysical parameters that best replicate the observed/ measured pressures and production and injection rates. The calibration of geomechanical stress modeling follows this exact concept.

The calibration of geomechanical models require a dataset that allows one to devolve a reliable indications of stress change. As stress changes cannot be directly measured stress calibration procedures rely on indirect indications of stress change: microseismicity; Interferometric Synthetic Aperture Radar (InSAR); seismic datasets, including inverted seismic velocities.

This current study focuses on the stepwise calibration of a hydromechanical simulation model through a VSP integration workflow. Several publications on the qualitative and quantitative utilization of seismic for improving hydrodynamic history matching (Huang et al., 1998) (Gosselin et al., 2003) has been found. Additionally, theoretical reviews which explore geomechanical calibration (Herwanger et al., 2005; Olden et al., 2001) driven by time-lapse datasets and manuscripts which address the building and initialization and 4D geomechanical modelling (Herwanger et al., 2011). This literature review focuses only on applications of hydromechanical calibration.

2.1 4D Geomechanical Calibration

“Microseismicity is a direct manifestation of mechanical deformation” (Verdon et al., 2011), allowing microseismic datasets to be used in stress history matching. Both Verdon and Chen use passive microseismicity to enhance the geomechanical understanding of their subject reservoirs. Verdon (2011) ground truths the Weyburn geomechanical model for the observed passive microseismicity occurrence and magnitude. Microseismicity is typically thought of as an injection-induced phenomenon, but the observed pattern deviated from this anticipated trend as the microseismicity occurrence clustered in the overburden above the producing wells. Reducing the reservoir stiffness by an order of magnitude lead to the replication of the observed micro-seismicity pattern and calibrated the model for this important indication of stress change.

Similarly, Chen et al. (2018) calibrated a fully coupled fluid flow-geomechanical simulation in Azle, Texas. The goal was to delineate the underlying cause of the regional microseismicity. The Azle Texas region has Barnett gas production, wastewater injection into the aquifer, which underlies the Barnett formation, and the regional microseismic events that occur near mapped faults. The authors used injection well bottom-hole-pressure (BHP) and cumulative microseismic moment to history match/ calibrate the fully coupled model. The study concluded that an imbalance of fluid influxes on opposing sides of the faults results in strain propagation and is the likely cause of the regional microseismicity.

Raziperchikolaee et al. (2021) utilized field data from the depleted carbonate reef studied by the Midwest Regional Carbon Sequestration Partnership to calibrate a poroelastic pressure-dependent model initially for a hydraulic fracture tests and subsequently for confirming the surface deformation in the observed InSAR datasets. As anticipated, depletion resulted in a negative time shift and conversely, the CO₂ injection re-inflated the storage compartment. Although relatively minuscule, the simulated uplifts compared well with the InSAR data indicating the calibration of the geomechanical model and allowing for more confident uplift predictions during the forecast phase.

In Salah is a well-known CCUS project in Algeria where the CO₂ is stripped from natural gas produced from the Krebka formation and reinjected into the formations' aquifer leg. Shi et al. (Shi et al., 2013) calibrated a coupled hydro-mechanical model over 5 years (2004-2009) (by modifying the Youngs Modulus) with the InSAR datasets for uplift over three horizontal CO₂ injector wells. The coupled model was built from a reservoir history match in which no CO₂ percolated from the Krebka to the overlying lower caprock via an existing vertical fault. One well (KB-501) showed an excellent match to the observed uplift dataset, while the matches to the remaining two wells were less impressive. This calibration study provides valuable information about the Krebka storage containment. It indicates that current model assumptions may need to be modified to achieve an improved match.

The concepts presented by Hatchell (2003) and Molenaar (2004) outline the geomechanical calibration for time-lapse time-steps using time-lapse- time shifts. Much of this work was inspired by the reservoir compaction, subsidence and the associated

overburden stretching experienced in stress-sensitive North Sea oil fields (Herwanger et al., 2005). Seismic amplitudes and inverted velocities can be used for 4D-Close-the-Loop (4D CtL) technologies which lead to hydromechanical calibration. 4D CtL drives towards improving reservoir and geomechanical characterization and informs future field development by reducing drilling risks and improving confidence in forecast predictions.

Nasser et al. (2018) have developed an iterative 4D-Close-the-Loop (4D CtL) process that forwards synthetic 4D seismic time-shifts using outputs from numerical simulation models and quantitatively compares these generated time-shift with observed time-shifts. Their work attempts to de-risk drilling operations in an HPHT field and focuses on assessing the two shale layers interbedded with two production zones. Shales are typically thought of as sealing; however, pressure diffusion over production time scales can result in changes in stresses which were detected in the seismic signature. Mismatches (RMS of the difference) between the observed and synthetic time-shifts are used to update reservoir and geo-mechanical parameters and drive the calibration process. Their work improves predictions of pore pressure profiles and stress tensor changes, better identifying high-risk formations and improving well planning.

Herwanger et al (2013) also calibrated a coupled hydro-mechanical model using time-lapse time-shifts. The subject reservoir requires hydraulic fracturing to achieve economic production rates. The goal of their study is to determine changes in stress orientation as this impacts the direction in which fractures are opened. Fractures open against the weakest direction, the minimum horizontal stress, but production and injection from nearby wells alter the local stress orientation (Bhardwaj et al., 2016; Yang et al., 2019). Time-lapse seismic acquisition used for geomechanical calibrations gave valuable insights into the required reorientation of production wells to achieve the desired fracture growth.

Similar to previously reviewed publications, this case study of the FWU field's science well uses time-lapse volumes to calibrate the coupled geomechanical model. Inherently, time-lapse records carry the combined effects of fluid substitution and subsurface pore pressure changes and utilize time-lapse seismic VSP inverted for seismic velocities (provided by LANL) as the observed dataset for the calibration. The VSP measurements were acquired around the 13-10A injector well.

Inherently, injection raises the near-wellbore pressure moving the stress state closer to both shear and tensile failure states, making the reservoir surrounding injectors more vulnerable for failure. More specifically, elevated pore pressure increases the shear stresses at the reservoir-caprock boundary (Hawkes, McLellan et al. 2005), and faults and fractures that are optimally oriented for reactivation become regions of increased geomechanical risks, even more so if they traverse the caprock.

Stress calibration, constrained by the VSP dataset, provides valuable insights into the Morrow B stress state evolution which is driven by local pressure perturbations. This current study benefits from laboratory ultrasonic seismic velocity measurements on core, which directly correlate between changes in mean effective stress and changes in seismic

velocity. The other factor that contributes to seismic velocity change is fluid substitution which is accounted for using a site-specific rock physics model with outputs of the compositional reservoir simulation.

The principal of superposition of seismic wave fields for fluid substitution and mean stress changes are implemented, allowing for the computation of modeled seismic velocities appropriate for comparison with the observed time-lapse seismic velocity dataset.

The following subsection presents the relevant theoretical background of the seismic wave equation and the link with geomechanics for an elastic isotropic mechanical model. Stiffness matrix coefficients are presented in terms of bulk and shear moduli. The theoretical background of the site-specific Krief rock physics model and the mean effective stress to seismic velocity relationship are also presented.

2.2 Stress and Strain, Concepts of Seismic Velocity Change

2.2.1 Linking Stress, Strain, and Seismic Wave Velocity

Seismic waves can be thought of as the propagation of energy through an elastic medium as it travels from its source. The seismic wave equation is the result of coupling of Newton's second law and stress-strain relationships given by,

$$\sigma_{ij,j}(x,t) = \rho \frac{\partial^2 u_i(x,t)}{\partial t^2} \quad (2.1)$$

where σ is the stress, ρ is density, t is time, and u is displacement. In an elastic medium, the Hooke's Law is defined by,

$$\sigma_{ij} = C_{ijkl} \varepsilon_{kl} , \quad (2.2)$$

where, $i, j, k = 1, 2, 3$ with Einstein summation convention. For an isotropic model the stiffness matrix has C_{ijkl} coefficients can be represented by two independent elastic moduli. Here because this project computes shear and compressional seismic velocity, the shear and bulk moduli are utilized. The Bulk modulus is material stiffness under hydrostatic compression and shear modulus relates applied shear stresses to the resulting shear strain.

$$C_{ijkl} = \begin{bmatrix} K + 4\mu/3 & K - 2\mu/3 & K - 2\mu/3 & 0 & 0 & 0 \\ K - 2\mu/3 & K + 4\mu/3 & K - 2\mu/3 & 0 & 0 & 0 \\ K - 2\mu/3 & K - 2\mu/3 & K + 4\mu/3 & 0 & 0 & 0 \\ 0 & 0 & 0 & \mu & 0 & 0 \\ 0 & 0 & 0 & 0 & \mu & 0 \\ 0 & 0 & 0 & 0 & 0 & \mu \end{bmatrix} \quad (2.3)$$

and ε_{kl} is defined as,

$$\varepsilon_{kl} = \frac{1}{2}(u_{k,l} + u_{l,k}). \quad (2.4)$$

Particle displacements for compressional seismic waves are parallel to propagation direction, while for shear seismic waves, particle displacements are perpendicular to the direction of propagation. Expressions for compressional P-wave seismic velocity (V_p) and shear S-wave seismic velocity are shown as equations 2.5 and 2.6, respectively,

$$V_p = \sqrt{\frac{K + \frac{4\mu}{3}}{\rho}}, \quad (2.5)$$

$$V_s = \sqrt{\frac{\mu}{\rho}}. \quad (2.6)$$

Shear and compressional seismic velocities are explicit functions of elastic moduli (saturated Bulk Modulus and Shear Modulus) and formation density both factors that are altered during the CO₂-WAG operations and which ought to impact measured observed seismic velocities.

2.2.2 Seismic Velocity: Impacts of Fluid Substitution

The Biot-Gassmann workflow (1956; 1951) models fluid effects on seismic velocities by computing the saturated elastic moduli and bulk formation density. The Biot Gassmann workflow's fundamental assumptions include clay-free, homogeneous, isotropic, fully saturated, and connected porous media. An additional assumption is that the acoustic waves propagate through the formation at low frequencies such that the seismic waves do not trigger pressure dis-equilibration within the pore spaces.

Equations 2.7, 8, 9 and 10 calculate the constituent elastic moduli and Bulk density for shear and compressional seismic velocity. The formation bulk density is the volume-weighted average of the rock matrix and fluid densities expressed in equation 2.7 (Batzle et al., 1992). Fluid density and saturation are extracted from the dynamic reservoir simulation model for each time-lapse time step. Equation 2.8 infers that the impact of changing pore fluids on the shear modulus is minuscule, and the saturated shear modulus to be set equal to the dry shear modulus.

We used the following equations 2.9 and 2.10 to determine the change in Bulk Modulus due to changes in fluid contents:

$$\rho_{Bulk} = \rho_{matrix}(1 - \phi) + \phi(\rho_o S_o + \rho_g S_g + \rho_w S_w), \quad (2.7)$$

$$\mu_{sat} = \mu_{dry}, \quad (2.8)$$

$$K_f = \frac{1}{c_f}, \quad (2.9)$$

$$K_{sat} = K_{fr} + \frac{\left[1 - \frac{K_{fr}}{K_s}\right]^2}{\frac{\phi}{K_f} + \frac{(1-\phi)}{K_s} - \frac{K_{fr}}{K_s^2}}, \quad (2.10)$$

where: ϕ is the matrix porosity, and S represents fluid saturation. The subscripts w, o, g represent water, oil, gas, respectively. K represents the bulk modulus with subscripts sat, fr, s, and f representing the saturated porous medium, the dry rock frame, the constituent solid grains, and the pore-filling fluid. c_f is the total fluid compressibility.

The saturated Bulk Modulus is the linear sum of the pore space's bulk moduli and the dry rock frame. The porosity, the solid constituent grain, dry rock frame, and the pore-filling Bulk Modulus all affect the saturated Bulk Modulus. Equation 2.9 shows that the fluid bulk modulus is computed at every time-lapse time-step from the total fluid compressibility extracted from the dynamic reservoir simulation model. Equation 2.10 is the final expression for the saturated Bulk Modulus of the porous medium.

2.2.3 Krief model Rockframe Elastic Moduli

The target formation, Morrow B is highly heterogenous due in part to dispersed clay deposited during its diagenetic evolution (Rose-Coss, 2017; Rose-Coss et al., 2015). Several studies have shown the unpredictable impacts of clay content on the Biot-Gassmann workflow results (Han et al., 1986; Tosaya, 1983; Vanorio et al., 2003). Consequently, the appropriate implementation of Biot Gassmann requires the development of a relationship between the properties of the rocks' composite grains and the rock frame, aptly expressed through the Biot poroelastic coefficient (2.11) (Geertsma (1957) and Skempton (1961)),

$$K_{fr} = (1 - \alpha) K_s. \quad (2.11)$$

This study benefits from a site-specific Krief rock physics model. Krief (1990) studied the relationships between elastic (Bulk Modulus and Shear Modulus) moduli and porosity for water-saturated sandstones (eq. 2.11), developing the following equation. The coefficient n is the linear tangent slope on the elastic moduli versus porosity plot, for Krief's study $n = 3$,

$$\alpha = 1 - [1 - \phi]^{\left(\frac{n}{1-\phi}\right)}. \quad (2.12)$$

Substitution of the Biot poroelastic coefficient into the eq 2.9 yields the equivalent expression for saturated bulk modulus given by

$$K_{sat} = K_{fr} + \frac{\alpha^2}{\frac{\phi}{K_f} + \frac{(\alpha-\phi)}{K_s}}. \quad (2.13)$$

2.2.4 Seismic Velocity to Mean Effective Stress: Impacts of Pore Pressure Change

Stress induced seismic velocity changes are an expression of the changing medium elasticity. For completeness, elasticity models relating seismic wave propagation to the changing stress state can be thought of in three categories:

1. Continuum mechanics approach considers a pre-stress state of the initial stress tensors (Sripanich et al., 2021; Tromp et al., 2018), allowing subsequent changes in stress to be related directly to pressure changes;
2. Third-order elasticity, which refers to the full 6-ranked tensor, with 56 independent parameters (Prioul et al., 2007; Worthington, 2008). Many practitioners utilize varying assumptions and arrangements of anisotropy to develop velocity-stress models for specific purposes.
3. Micromechanical models relate to classical excess compliance introduced by Sayer and Kachanov (1995).

This current study uses a micromechanical model. Shear and compressional seismic velocities are affected by changes in subsurface pore pressure. The reservoir is a poroelastic medium on which imposed loads can deform the connected pore spaces, the rock matrix's fabric, or both. The reservoirs' rock matrix is restricted from volume deformation by the surrounding tectonic forces. Consequently, modifications to the pore pressure affect the normal stresses applied to the inside of the pore surfaces: dilation for pore pressure increase and contraction for pore pressure decrease. Essentially, the pore pressure bears a portion of any imposed load (Biot, 1955),

$$\sigma'_{ij} = \sigma_{ij} - \alpha \delta_{ij} P, \quad (2.14)$$

where, σ'_{ij} is the effective stress, α is the poroelastic Biot coefficient, which scales the impact of the pressure pore (P) change.

Expanded or contracted pore space ultimately impacts the bulk density and the Bulk Modulus of the formation through which the seismic waves travel. These property modifications inherently cause changes to the shear and compressional seismic velocities as they impact the stiffness matrix. This link between pore pressure changes, stress changes, and seismic velocity changes is well known (Birch 1961, Nur and Simmons 1969). It has been thoroughly explored by laboratory studies (Eberhart-Phillips, Han, et al. 1989, Mese 2005). The laboratory studies utilize a confining pressure akin to the overburden pressure. The opposing effects of confining pressure and pore pressure align with Equation 2.13. Empirical relationships between seismic velocity and stress have been devised (Dobróka and Molnár 2012). This study of the ongoing CO₂ WAG operations within the Morrow B benefit from similar ultrasonic measurements, thereby relating changes in effective pressure to shear and compressional seismic velocity.